Article

Highly Efficient Au/ZnO−ZrO$_2$ Catalysts for CO Oxidation at Low Temperature

Roberto Camposeco, Viridiana Maturano-Rojas and Rodolfo Zanella *

Instituto de Ciencias Aplicadas y Tecnología, Universidad Nacional Autónoma de México, Circuito Exterior S/N, C. U., Mexico City 04510, Mexico; roberto.camposeco@icat.unam.mx (R.C.); viridiana.maturano@icat.unam.mx (V.M.-R.)

* Correspondence: rodolfo.zanella@icat.unam.mx

Abstract: A series of gold catalysts on ZnO−ZrO$_2$ featuring nominal ZnO loads of 3, 5, and 10 wt. % were synthesized by the sol–gel method using Zn(NO$_3$)$_2$ and zirconium (IV) propoxide aqueous solutions. In addition, gold catalysts with nominal loads between 1 and 3 wt. % were produced by the method of deposition-precipitation with urea, and their performance in the CO oxidation reaction at low temperature was evaluated. HRTEM outcomes revealed high gold dispersion on the 3Au/5ZnO−ZrO$_2$ catalyst with Zn/Zr atomic ratio of (5/95) and 3 wt. % of gold, which showed the highest CO conversion at low temperature (−5 °C) under air treatment when the CO oxidation was carried out with a space velocity of ~46,000 h^{-1}. The incorporation of ZnO to ZrO$_2$ provoked high dispersion of the gold nanoparticles on the support and close size distribution; moreover, the presence of Au^{1+} and Zr^{3+} species was increased by the Zr−O−Zn interaction, which was stronger than in the single Au/ZrO$_2$ and Au/ZnO catalysts. DRIFT/GC−MS confirmed that the Au^{1+}/Au^0 ratio and formation of carbonate species played an important role in determining the CO conversion; likewise, the 3Au/5ZnO–ZrO$_2$ catalyst was stable at 10 °C for 24 h.

Keywords: ZnO−ZrO$_2$; CO oxidation; nanoparticles; gold catalyst

1. Introduction

Gold catalysts on reducible metal oxides have shown outstanding performance in oxidizing CO to CO$_2$ [1]. In this sense, dispersed gold nanoparticles on metal oxides have been investigated due to their ability to provide reactive oxygen coming from the metal oxide [2], where TiO$_2$, CoO$_x$, CeO$_2$, and Fe$_2$O$_3$ have exhibited high catalytic activity in CO oxidation [3]. There are many factors that influence the CO oxidation, such as strong gold particles–support contact, gold particle size, and support type (either reducible or non-reducible). In this context, techniques of deposition-precipitation with urea stand out in producing a strong interaction between gold nanoparticles (average gold particle size 1–3 nm) and support [4,5]. As for metal oxides, the interaction between zinc oxide and gold should get more attention in order to be better understood, mainly because of the non-reducible behavior of ZnO; in addition, the dispersion and interaction between gold nanoparticles and ZnO is not high. However, there are some reactions catalyzed by gold nanoparticles supported on ZnO, such as methanol synthesis, selective catalytic reduction of NO using propene, and photocatalytic reactions [6]; furthermore, Au/ZnO has been proven to achieve high selectivity towards methanol and reduce methane formation in CO hydrogenation [6,7]. Nevertheless, scarce data are available on the synthesis of Au/ZnO catalysts [8]. The preparation method that has mainly been described in the literature so far is co-precipitation [9]. On the other hand, although ZnO is not a reducible oxide, good activity and stability in the CO oxidation have been made possible by Au/ZnO materials [10]. A study of gold supported on ZnO and TiO$_2$ proposed the existence of two kinds of metallic gold sites: terrace and particle borderline sites, which can adsorb both oxygen and carbon monoxide at the same time [11]. Earlier

research on Au/ZnO catalysts has reported good catalytic activity and stability in the CO oxidation at room temperature in the presence of H_2O [12,13]. Au/CuO, Au/ZnO, and Au/CuO–ZnO materials synthesized by the co-precipitation method were highly active in CO oxidation and stable at 20 °C. The best performance was displayed by Au/ZnO featuring the smallest and most homogeneously dispersed Au nanoparticles (2–5 nm), in comparison with other catalysts [14]. In this way, even though $ZnO-ZrO_2$ has been studied as a support catalyst in some oxidation reactions, no studies have been reported on the performance of gold dispersed on the $ZnO-ZrO_2$ system in the CO oxidation reaction at low temperature.

The study reported here investigated the activity–structure relationship of a series of Au/ZnO–ZrO_2 materials in CO oxidation. The properties of single ZrO_2 were improved by adding ZnO. It is shown that the proportion of hydroxyl groups, the carbonate species, and the surface area influenced the catalytic properties of gold nanoparticles as well as their dispersion. The objective of the present research was to find the optimal loadings of gold and ZnO on ZrO_2 as catalysts, containing ZrO_2 as the main component phase, to perform the low-temperature CO oxidation reaction and elucidate the factors that affect the catalytic performance of these materials. It is proposed that the strong $Zn-O-Zr$ interaction and good gold dispersion may explain the enhanced performance in the CO oxidation displayed by the Au/ZnO–ZrO_2 catalysts, which is in contrast with the single Au/ZnO and Au/ZrO_2 catalysts.

2. Results

2.1. Crystalline Structure

The X-ray diffraction technique (XRD) was used to identify crystalline phases in the 3Au/ZrO_2, 3Au/ZnO, and 3Au/5ZnO$-ZrO_2$ catalysts, as well as to obtain the mean crystallite sizes in the materials. Figure 1 displays the XRD patterns of the 3Au/ZrO_2, 3Au/ZnO, and 3Au/5ZnO$-ZrO_2$ catalysts. The XRD pattern of the prepared crystalline 3Au/ZnO is in accordance with the thermodynamically stable hexagonal wurtzite structure of ZnO (JCPDS card No. 36-1451). For 3Au/ZrO_2, the peaks located at 2θ = 30.2°, 35.2°, 50.7°, 31.57°, 60.2°, 62.8°, and 74.5° correspond to the (1 1 0), (1 1 0), (2 2 0), (2 1 1), (2 0 2), and (2 0 0) crystal planes of the tetragonal structure of ZrO_2 (JCPDS card No. 79-1769, with P42/nmc space group). The 3Au/5ZnO$-ZrO_2$ catalysts show tetragonal crystalline structure, while for the hexagonal wurtzite structure of ZnO, no peaks are clearly detected. In addition, peaks located at 2θ = 30.2°, 35.2°, 50.7°, 31.57°, 60.2°, 62.8°, and 74.5° correspond to the (1 1 0), (1 1 0), (2 2 0), (2 1 1), (2 0 2), and (2 0 0) crystal planes of the tetragonal structure of ZrO_2 (JCPDS card No. 79-1769, with P42/nmc space group). No peaks were observed for gold according to the JPDCS card No. 04-0784 due to its high dispersion in the three different ZnO, ZrO_2, and $ZnO-ZrO_2$ catalyst supports. On the other hand, in Figure 1, it is evidenced that although 5 wt. % of ZnO was incorporated into ZrO_2, the crystallite size was not modified (Table 1); this fact was corroborated by the Scherrer equation. Table 1 shows that the surface area of the 3Au/5ZnO$-ZrO_2$ sample increased to 157 m^2/g with respect to 95, and 59 m^2/g for the 3Au/ZrO_2 and 3Au/ZnO samples, respectively. Therefore, this outcome revealed that the presence of ZnO on ZrO_2 allowed improvement of the textural and structural properties of the material.
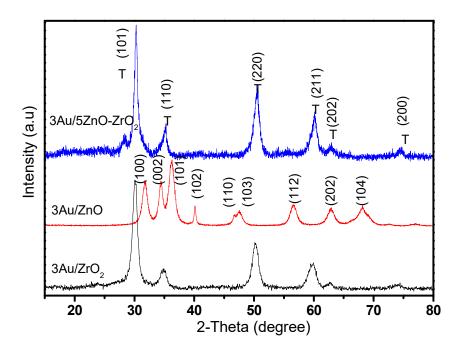
Figure 1. XRD patterns of the 3Au/ZrO$_2$, 3Au/ZnO, and 3Au/5ZnO$-$ZrO$_2$ catalysts.
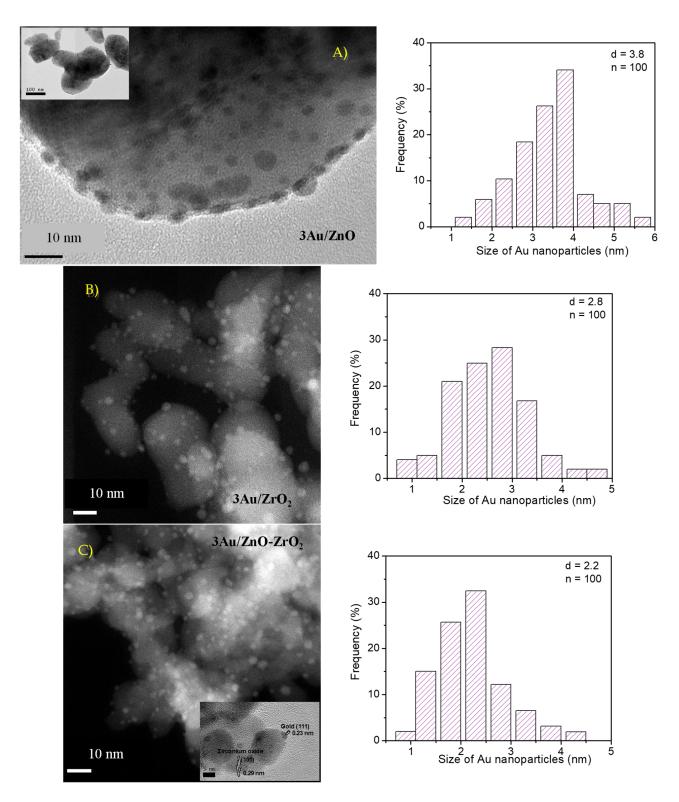
Table 1. Properties of the 3Au/ZrO$_2$, 3Au/ZnO, and 3Au/5ZnO$-$ZrO$_2$ catalysts annealed at 200 °C under air atmosphere, as well as kinetic data regarding the CO oxidation reaction.

Property	3Au/ZrO$_2$	3Au/ZnO	3Au/5ZnO$-$ZrO$_2$
Nominal Au content, wt. %	3	3	3
Actual Au content, wt. %	2.85	2.7	2.92
S$_{BET,}$ m^2/g	95	59	157
Crystallite size, nm	10	18	12
Activation energy (Ea), kJ/mol	33.6	48.5	21.7
Au particle size, nm	2.8	3.5	2.2
Au dispersion, %	48	38	56
Rate, mol$_{CO}$/mol$_{Au}$•s *	0.003	0.0015	0.006
Turnover frequency, TOF (h^{-1}) *	38	12.4	70.4

* TOF and reaction rates were calculated at 5 °C under kinetic conditions, at conversions of CO below 18%.

2.2. Morphology

The TEM image of 3Au/ZnO reduced with air at 200 °C shows that the catalyst consists of highly aggregated lumps whose size is mainly between 20 and 30 nm (see inset in Figure 2A). The gold particles presented an average particle size of 3.5 nm, and Au is also observed at the edge of the Zn crystalline structures. In this way, non-homogeneous particles with different sizes are shown in the HAADF/STEM image of 3Au/ZrO$_2$ (see Figure 2B), and small gold particles with average size of 2.8 nm are evidenced in the regions with different particle sizes of ZrO$_2$ (Figure 2B). In the HAADF/STEM image of the 3Au/5ZnO$-$ZrO$_2$ catalyst (Figure 2C), Au and Zr are mainly revealed, which is confirmed by the HRTEM technique inset in Figure 2C (see Figure S1 in the Supplementary Materials), with highly dispersed gold nanoparticles with an average particle size of 2.2 nm. Au nanoparticles mainly present on a bulk of ZnO$-$ZrO$_2$ structures can be seen in Figure 2C.
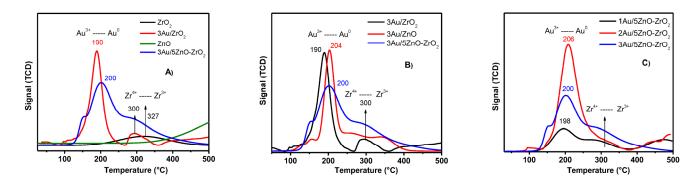
Figure 2. (**A**) HRTEM images of the 3Au/ZnO catalyst annealed at 200 °C in air and its corresponding crystal size frequency histogram, (**B**) HAADF/STEM images of the 3Au/ZrO$_2$, and (**C**) 3Au/5ZnO−ZrO$_2$ catalysts and their corresponding particle size frequency histograms.

2.3. Reducibility of the Catalysts

The reduction behavior of the catalysts was explored by hydrogen temperature programmed reduction (H$_2$-TPR) of the 3Au/ZrO$_2$, 3Au/ZnO, and 3Au/5ZnO−ZrO$_2$ catalysts. As shown in Figure 3A–C, all the catalysts exhibit a broad band in the 100–400 °C

interval; in this way, it is known that ZnO and ZrO_2 are not reduced at temperatures below 300 °C, so the first reduction peak is assigned mainly to the reduction of well-dispersed gold species [14–17]. As shown in Figure 2A, ZnO did not present reduction peaks at low temperature due to its high thermal stability. The broad peak with its maximum at 327 °C is ascribed to the reduction of coordinatively unsaturated Zr^{4+} species at the ZrO_2 surface. The maximum of this peak is slightly shifted to a lower temperature (300 °C) in the Au/ZrO_2 sample compared to the bare ZrO_2 (327 °C; see Figure 3A), which suggests that the presence of Au species promotes the redox properties of $3Au/ZrO_2$; this outcome reveals the possibility of zirconium reduction in ZrO_2. Likewise, the addition of zinc oxide and gold to ZrO_2 provoked a strong surface reduction, which also improved the interaction between the species in the $3Au/5ZnO-ZrO_2$ sample, notably widening the reduction peak between 100 and 400 °C with respect to the monometallic counterparts that showed sharper reduction peaks. On the other hand, the addition of gold nanoparticles to $ZnO-ZrO_2$ produced a peculiar surface reduction peak shift towards lower temperatures with regard to the sample without gold. The temperatures of maxima of gold reduction peaks increased as follows: $3Au/ZnO > 3Au/5ZnO-ZrO_2 > 3Au/ZrO_2$. On the other hand, slight differences in the reduction behavior of $5ZnO-ZrO_2$ with different gold loadings are observed, with the maximum of gold reduction at 198 °C for the sample containing 1 wt. % of Au and 206 °C for the sample containing 2 wt. %, while it occurred at 200 °C for the 3 wt. % sample (see Figure 3C). In addition, from Figure 3C, it can be observed that the reduction capacity of gold is displayed by a more intense peak in the $2Au/5ZnO-ZrO_2$ catalyst than in $1Au/5ZnO-ZrO_2$ and $3Au/5ZnO-ZrO_2$. In this sense, it seems that the $2Au/5ZnO-ZrO_2$ catalyst possesses a better hydrogen dissociation ability than the $1Au/5ZnO-ZrO_2$ and $3Au/5ZnO-ZrO_2$ samples; this fact was also reflected in the catalytic activity (see Catalytic Activity section below). When the catalysts were thermally treated in H_2 atmosphere, the $2Au/5ZnO-ZrO_2$ catalyst showed lower T_{90} than those of $1Au/5ZnO-ZrO_2$ and $3Au/5ZnO-ZrO_2$, but not when the catalysts were thermally treated in air at the same temperature. It is also suggested that the metal–support interaction was higher in the $3Au/5ZnO-ZrO_2$ catalyst, evidenced by a wider reduction peak, compared to the $2Au/5ZnO-ZrO_2$ one.
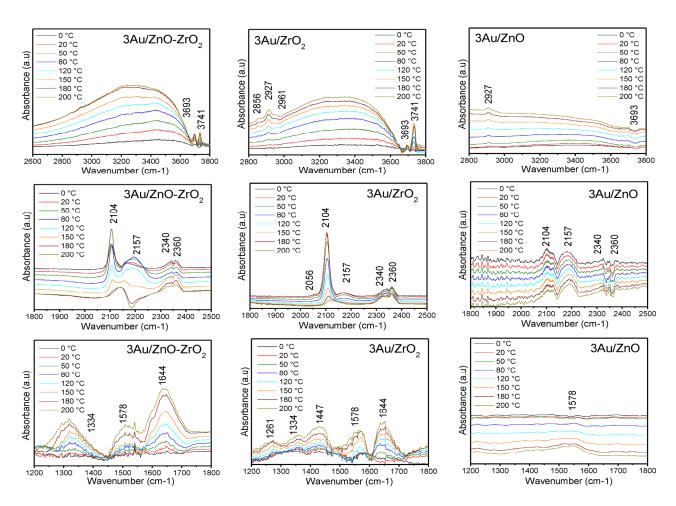

Figure 3. (**A**) Reduction profiles for the ZrO_2, ZnO, $3Au/ZrO_2$, and $3Au/5ZnO-ZrO_2$ catalysts. (**B**) Reduction profiles for the $3Au/ZrO_2$, $3Au/ZnO$, and $3Au/5ZnO-ZrO_2$ catalysts. (**C**) Reduction profiles for the $1Au/5ZnO-ZrO_2$, $2Au/5ZnO-ZrO_2$, and $3Au/5ZnO-ZrO_2$ catalysts.
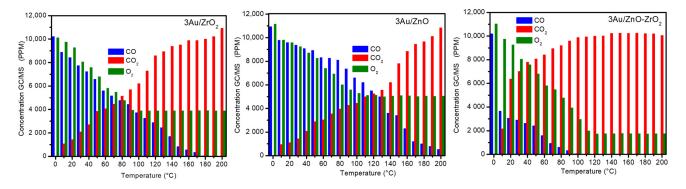
2.4. DRIFTS CO Oxidation

DRIFTS analyses were carried out to study the evolution and interaction between gold and ZnO or ZrO_2 species using a CO probe molecule (Figure 4). It is noted that CO was adsorbed on the $3Au/ZrO_2$, $3Au/ZnO$, and $3Au/5ZnO-ZrO_2$ catalysts from RT, showing two feature bands, identified at ~2157 and ~2104 cm^{-1}; the first one has been related to CO adsorbed on Zr^{4+}, which is a characteristic of the Lewis acid site from tetragonal ZrO_2; however, this band can also be associated with CO in gas phase. In the same way, it was observed for the Au/ZnO catalyst, where the CO vibrational band

located at ~2104 cm^{-1} was detected and assigned to CO molecules linearly adsorbed onto Au^0 species displaying higher intensity in the $3Au/ZrO_2$ and $3Au/5ZnO-ZrO_2$ catalysts than in the $3Au/ZnO$ catalyst (see Figure 4) [18,19]. The bands observed at ~2300–2400 cm^{-1} correspond to CO_2 species. On the other hand, several carbon-related species in the frequency region from 1800 to 1200 cm^{-1} were observed in the $3Au/ZrO_2$, $3Au/ZnO$, and $3Au/5ZnO-ZrO_2$ catalysts. CO_3^{2-} species at ~1250–1300 and ~1581 cm^{-1}, and mono-dentate carbonate species (CO_3^{2-}) at ~1300–1400 cm^{-1} are observed [19]. The bands located at ~1296 and ~1581 cm^{-1} were assigned to the strong and antisymmetric vibrations of bi-dentate CO_3^{2-} species, whereas the band identified at ~1388 cm^{-1} was related to the vibration of mono-dentate carbonate species according to [2,20,21]. Moreover, the band observed at ~1248 cm^{-1} was related to the presence of the asymmetric vibration of HCO_3^- due to the interaction between CO molecules and gold nanoparticles, as well as to surface OH groups of the $ZnO-ZrO_2$ mixed oxide [2,22]. In parallel, the bands at ~1581 and ~1296 cm^{-1} are assigned to carbonate bi-dentate species [23]. Additionally, when the temperature was increased to 140 °C, the band at about ~2086 cm^{-1} gradually disappeared. However, the presence of bicarbonate species on the catalyst surface observed at ~1248 cm^{-1} slightly decreased, while bi-dentate carbonate species at ~1550–1600 cm^{-1} remained unchanged in agreement with earlier literature [2,23,24]. It is also evidenced that HCO_3^- species were decomposed into CO_2 from RT, while the decomposition of CO_3^{2-} species into CO_2 occurred at higher temperature. Based on the results of the present work and those of previously reported studies [20–23], it is suggested that the oxidation pathway of CO on the surface of the $3Au/ZrO_2$, $3Au/ZnO$, and $3Au/5ZnO-ZrO_2$ catalysts could take place as follows: after the fast evolution of CO into various carbon species, the transformation of bicarbonate species into CO_2 as well as the decomposition of b-CO_3^{2-} and m-CO_3^{2-} species into CO_2 may proceed at the same time, mainly in the $3Au/ZrO_2$ and $3Au/5ZnO-ZrO_2$ catalysts with respect to the $3Au/ZnO$ catalyst, as can be observed in Figure 4. On the other hand, in the spectra in the 3800–2800 cm^{-1} region for the $3Au/5ZnO-ZrO_2$, $3Au/ZrO_2$, and $3Au/ZnO$ catalysts, two kinds of OH stretching bands are observed at ~3665 and ~3730 cm^{-1} in all the catalysts. The low intensity band at ~3693 cm^{-1} is related to hydrogen bound to adjacent OH groups, whereas the band at ~3741 cm^{-1} is assigned to isolated OH groups [4,25]. It was observed that when the temperature was raised from RT to 200°C, H_2O molecules were removed, and the bands located at 3000–3500 cm^{-1} decreased in intensity; in the same way, the magnitude of the bands located at 1400–1600 cm^{-1} also decreased. It was noticed that the ability to produce OH groups and absorb H_2O followed the order: $3Au/5ZnO-ZrO_2$ > $3Au/ZrO_2$ > $3Au/ZnO$. The outcomes by DRIFTS showed that the interaction between Au and ZnO or ZrO_2 or $ZnO-ZrO_2$ outstandingly modified the adsorption properties of the catalyst surface, revealing that the presence of carbonate species (1200–1600 cm^{-1}) in the $3Au/5ZnO-ZrO_2$ and $3Au/ZrO_2$ catalysts, with regard to the $3Au/ZnO$ catalyst, could represent an overriding key step in the catalytic oxidation of carbon monoxide (as seen in Figure 4), which seems to be related to the highly active CO oxidation (see the section about catalytic activity results below). On the other hand, the evolution of gases outside the DRIFTS cell was analyzed by GC–MS. Figure 5 shows the relative CO_2 yields for $3Au/ZrO_2$, $3Au/ZnO$, and $3Au/5ZnO-ZrO_2$ in air treatments at 200 °C as functions of time for each temperature within this overall experiment. The CO and O_2 reactions revealed the enhancement of the CO_2 yield when the temperature was increased from RT up to 200 °C for all the catalysts. In all the cases, over the investigated temperature interval, the CO_2 yield grew, being more evident for the $3Au/5ZnO-ZrO_2$ catalyst than for $3Au/ZrO_2$ and $3Au/ZnO$.

Figure 4. In situ DRIFTS spectra for the $3Au/ZrO_2$, $3Au/ZnO$, and $3Au/5ZnO-ZrO_2$ catalysts in the CO oxidation from RT to 200 °C at different wavenumber intervals: $3800-2200$, $3800-2800$, and $1200-1800$ cm^{-1}.

Figure 5. GC/MS profiles for the $3Au/ZrO_2$, $3Au/ZnO$, and $3Au/5ZnO-ZrO_2$ catalysts in the CO oxidation from RT to 200 °C.
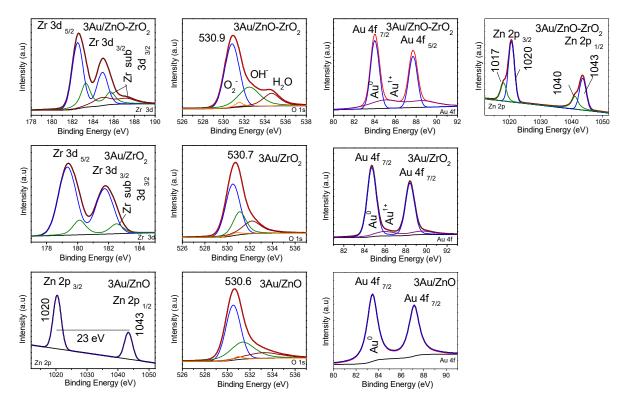
2.5. Surface Evolution by XPS

X-ray photoelectron spectroscopy (XPS) outcomes shown in Figure 6 display the Zr 3d spectra for the $3Au/ZrO_2$ and $3Au/5ZnO-ZrO_2$ catalysts thermally treated in air at 200 °C. Both catalysts displayed a doublet with a spin-orbit splitting of 2.4 eV corresponding to Zr $3d_{5/2}$ at ~182.2 eV [26]. The profiles of the $3Au/ZrO_2$ and $3Au/5ZnO-ZrO_2$ catalysts treated with air at 200 °C were quite similar; the main difference observed between the bimetallic catalysts and the monometallic one is the interaction and splitting related to zirconium sub-oxide species observed towards higher binding energies at 188 eV. In this

sense, the displayed Zr 3d peak is very broad, indicating the occurrence of other Zr species. Moreover, the spectra indicate the existence of zirconium mainly as Zr^{4+} species on the $3Au/ZrO_2$ catalyst accompanied by a small proportion of sub-oxide Zr^{3+} (see Figure 5). In addition, the Zr 3d spectra for the $3Au/ZrO_2$ and $3Au/5ZnO-ZrO_2$ catalysts show two peaks ascribed to Zr $3d_{5/2}$ and Zr $3d_{3/2}$. In the spectra of the $3Au/5ZnO-ZrO_2$ catalyst, the peaks of Zr $3d_{5/2}$ ~183.63 and ~181.37 eV were fitted to Zr^{3+} and Zr^{4+} species, respectively, showing a spin-orbit splitting value of 2.3 eV. On the other hand, Figure 6 shows the XPS spectra for the Zn 2p region of the $3Au/ZnO$ and $3Au/5ZnO-ZrO_2$ catalysts, where double peaks are observed in the Zn 2p spectra, with main B.E. at 1043 and 1020 eV and spin-orbit coupling energy of 23 eV. The peaks are ascribed to $Zn_{2p1/2}$ and $Zn_{2p3/2}$ lines, respectively; the B.E. reveals two peaks from 1020 to 1023 eV and from 1040 to 1043 eV for the $Zn_{2p3/2}$ and $Zn_{2p1/2}$ lines, respectively, suggesting that Zn^{2+} on the surface was slightly modified after the addition of zinc to zirconium in the $3Au/5ZnO-ZrO_2$ catalyst [27]. Every peak is well fitted by the deconvolution with two peaks. In this way, the peaks at 1020 and 1043 eV are earmarked to zinc in tetrahedral sites in spinel lattices, and the peaks at 1017 and 1040 eV are allocated to zinc at octahedral sites in spinel lattices [28]. By the addition of Zn to Zr, the intensity of the Zn 2p spectra, assigned to octahedral sites in zinc spinel lattices, was increased. This fact shows that the wurtzite phase defects associated with octahedral zinc remained in the ZnO-ZrO_2 mixed oxide; however, the concentration of octahedral zinc defects increased by the addition of Zn to zirconia crystals [3,29]. The Au 4f peaks at B.E values of ~83.9 and ~84.4 eV are associated with Au^0 species. A typical Au 4f spectrum for the $3Au/ZrO_2$, $3Au/ZnO$, and $3Au/5ZnO-ZrO_2$ catalysts is shown in Figure 6. The curve fitting of the Au 4f spectra is mainly carried out with the spin-orbit splitting value of 3.7 eV [30]. The Au 4f curve fitting of the $3Au/ZrO_2$, $3Au/ZnO$, and $3Au/5ZnO-ZrO_2$ catalysts is shown in Figure 6. It is observed that two Au $4f_{7/2}$ components at B.E. of 84.5 and 85.8 eV are related to Au^0 and Au^1 species, respectively. Outcomes revealed the presence of Au^{1+} species, whose relative concentration is shown in Table 2. Au^0 species are present in the $3Au/ZrO_2$, $3Au/ZnO$, and $3Au/5ZnO-ZrO_2$ catalysts as nanoparticles (2–3 nm), which were not detected by X-ray diffraction. Moreover, the deconvolution for oxygen 1s of the $3Au/ZrO_2$, $3Au/ZnO$, and $3Au/5ZnO-ZrO_2$ catalysts mainly shows three and four peaks, while the one at ~530.1 eV is due to lattice oxygen on ZrO_2, the one at ~ 531.1 eV is attributed to OH groups, and the one at ~532.5 eV is assigned to the presence of H_2O [31]. Moreover, the additional peak at ~531.5 eV is related to metal-bound oxygen, which was observed in all the catalysts.

2.6. Catalytic Activity

Figure 7A shows the results of CO conversion as a function of the reaction temperature for the $3Au/ZrO_2$, $3Au/ZnO$, and $3Au/5ZnO-ZrO_2$ catalysts treated at 200 °C under air atmosphere. The $Au/5ZnO-ZrO_2$ catalyst showed higher catalytic activity with respect to the $3Au/ZrO_2$ and $3Au/ZnO$ catalysts (Figure 7A and Table 1); the addition of 3 wt. % of gold to $Au/5ZnO-ZrO_2$ increased the CO oxidation at −5 °C (87% of conversion), achieving a T_{90} of 5 °C (temperature to reach 90% of conversion) at 150 °C, whereas for Au/ZrO_2, 12% of conversion was reached at −5 °C, and the T_{90} was of 178 °C. For the $3Au/ZnO$ catalyst, 11% of conversion was achieved at 20 °C, and the T_{90} was possible at 260 °C. On the other hand, when the $3Au/ZrO_2$, $3Au/ZnO$, and $3Au/5ZnO-ZrO_2$ catalysts were treated at 200 °C under H_2 atmosphere, the $Au/5ZnO-ZrO_2$ catalyst continued exhibiting superior catalytic activity with regard to the $3Au/ZrO_2$ and $3Au/ZnO$ catalysts (Figure 7B). The $Au/5ZnO-ZrO_2$ catalyst increased the catalytic oxidation at −5 °C (78% of conversion), showing a T_{90} value of 66 °C, whereas for the Au/ZrO_2 catalyst, 21% of conversion was achieved at −5 °C, and a T_{90} value of 155 °C was noted. The $3Au/ZnO$ catalysts presented 17% of conversion at 20 °C and a T_{90} value of 170 °C. Moreover, the catalytic performance displayed by the $3Au/ZrO_2$, $3Au/ZnO$, and $3Au/5ZnO-ZrO_2$ catalysts was affected by the different atmospheres (air or H_2). It is interesting to note that the $3Au/5ZnO-ZrO_2$ catalyst thermally treated at 200 °C in air was more active than

the one thermally treated in H_2 at 200 °C, while the $3Au/ZrO_2$ and $3Au/ZnO$ catalysts showed higher CO conversions when they were activated in hydrogen. Table 3 summarizes the temperatures required to achieve 10, 50, or 90% of CO conversion (T_{10}, T_{50}, and T_{90}, respectively) for the different catalysts studied here, activated under air or under hydrogen atmosphere at 200 °C.

Figure 6. X-ray photoelectron spectra of the zinc Zn 2p, zirconium Zr 3d, oxygen O1s, and gold Au 4f deconvolution for the $3Au/ZrO_2$, $3Au/ZnO$, and $3Au/5ZnO-ZrO_2$ catalysts at 200 °C in air.

Table 2. Deconvolution outcomes for O 1s and Au 4f species of the $3Au/ZrO_2$, $3Au/ZnO$, and $3Au/5ZnO-ZrO_2$ catalysts activated at 500 °C.
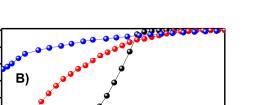
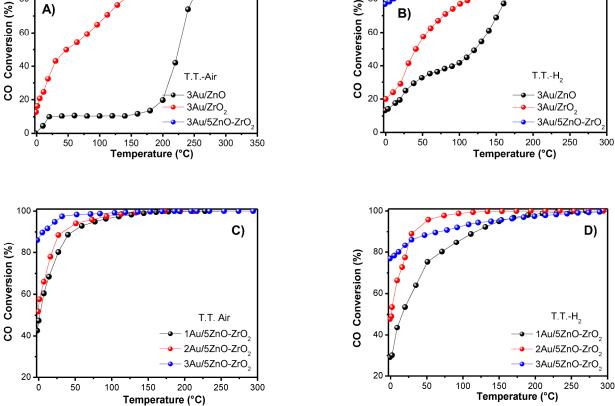| Catalyst	Au^0 (% Atom)	Au^{1+} (% Atom)	$O_{I(S-O)}$ (% Atom)	$O_{II(O-H)}$ (% Atom)	$O_{III(H_2O)}$ (% Atom)	$O_{IV(M-O)}$ (% Atom)
$3Au/ZrO_2$	87	13	47	30	23	0
$3Au/ZnO$	100	0	55	20	18	5
$3Au/5ZnO-ZrO_2$	84	26	49	27	15	7

Table 3. Reaction temperature comparison to achieve 10, 50, or 90% of CO conversion of the different catalysts activated at 200 °C under air and H_2 thermal treatments.

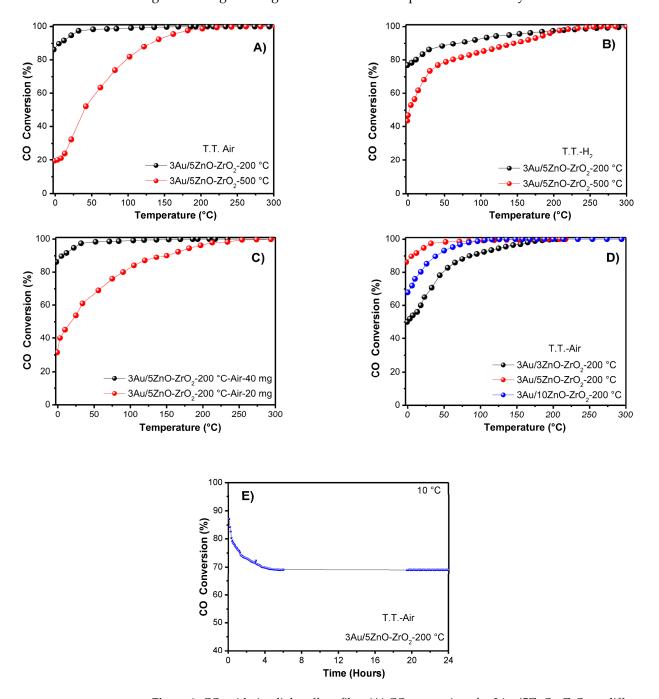| Catalyst	$T_{10\,Air}$	$T_{50\,Air}$	$T_{90\,Air}$	$T_{10\,H2}$	$T_{50\,H2}$	$T_{90\,H2}$
$3Au/ZrO_2$	−5	45	178	<−5	43	155
$3Au/ZnO$	18	220	260	−5	120	170
$1Au/5ZnO-ZrO_2$	<−5	1	47	−5	16	117
$2Au/5ZnO-ZrO_2$	<−5	−1	30	<−5	2	32
$3Au/5ZnO-ZrO_2$	<−5	<−5	5	<−5	<−5	66
$3Au/3ZnO-ZrO_2$	<−5	−3	83	–	–	–
$3Au/10ZnO-ZrO_2$	<−5	<−5	36	–	–	–

Figure 7. Temperature profiles and performance displayed by the tested catalysts: (**A**,**B**) comparison of CO conversions as functions of the reaction temperature for the $3Au/ZrO_2$, $3Au/ZnO$, and $3Au/5ZnO−ZrO_2$ catalysts, GHSV of 46,000 h−1, treated under air or H_2 atmosphere at 200 °C; comparison of CO conversions for the $1Au/5ZnO−ZrO_2$, $2Au/5ZnO−ZrO_2$, and $3Au/5ZnO−ZrO_2$ catalysts with different gold loadings (1, 2, and 3 wt. %) using thermal treatments under air (**C**) or hydrogen (**D**) atmosphere at 200 °C and GHSV of 46,000 h−1.

2.6.1. Effect of Pretreatment Gas and Gold Loading

Figure 7C,D show the light-off CO oxidation curves for the $5ZnO−ZrO_2$ sample, varying the gold loading at 1, 2, and 3 wt. % for the samples thermally treated under air atmosphere at 200 °C, respectively. All the catalysts thermally treated at 200 °C under air or H_2 showed better catalytic performance than the ones thermally treated under H_2. The CO conversion of the $1Au/5ZnO−ZrO_2$ catalyst thermally treated at 200 °C was 42% at −5 °C, showing a T_{90} value of 47 °C; the $2Au/5ZnO−ZrO_2$ catalyst displayed 52% CO conversion at −5°C, and a T_{90} value of 30 °C, whereas for the $3Au/5ZnO−ZrO_2$ catalyst, the CO conversion was 87% at −5 °C, showing a T_{90} value of 5 °C when treated in air atmosphere. On the other hand, when the samples were thermally treated in hydrogen at 200 °C, the $1Au/5ZnO−ZrO_2$ catalyst showed a CO conversion of 28% at −5 °C, and a T_{90} value of 117 °C; for the $2Au/5ZnO−ZrO_2$ catalyst, the CO conversion at −5 °C was 49%, showing a T_{90} value of 32 °C; with regard to $3Au/5ZnO−ZrO_2$, it displayed 78% CO conversion at −5 °C, and a T_{90} value of 66 °C. It should be noted that the thermal treatment in air or H_2 had a significant impact on the $Au/ZnO−ZrO_2$ catalyst behavior. In fact, some previous works on the catalytic activity of gold particles supported on oxides in the oxidation of CO have shown that the catalytic activity depends on both the annealing temperature and atmosphere used during the thermal treatment. In this way, the gold particles deposited on the $5ZnO−ZrO_2$ support, synthesized by the deposition-precipitation

method, grew when the annealing temperature increased, making the catalysts less active, in agreement with [32]. Therefore, the highest activity at 200 °C under air and hydrogen thermal treatments may be related to the high dispersion of gold nanoparticles, mainly in the 5ZnO−ZrO$_2$ support (see Figure 8 and Table 1; for more information, see the Supporting Information, Figure S2). The addition of ZnO to ZrO$_2$ allowed the stabilization of the gold nanoparticles at 200 °C. Thus, the activation of the catalysts is essential for the CO oxidation reaction, showing that the CO oxidation increased after activation at 200 °C (see Figure 7). Moreover, it is observed that thermal treatment in air produces a more active catalyst than a thermal treatment in hydrogen (Figure 7C,D) and that the conversion increased as the gold loading was augmented when the samples were thermally treated in air.

Figure 8. CO oxidation light-off profiles: (**A**) CO conversions for 3Au/5ZnO−ZrO$_2$ at different temperatures (200 and 500 °C), treated under air atmosphere, GHSV of 46,000 h−1; (**B**) CO conversions

for 3Au/5ZnO−ZrO$_2$ at different temperatures (200 and 500 °C), under H$_2$ atmosphere, GHSV of 46,000 h−1; (**C**) CO conversions for 3Au/5ZnO−ZrO$_2$ for 40 and 20 mg of catalysts, treated under air atmosphere; (**D**) comparison of CO conversions for the 3Au/3ZnO−ZrO$_2$, 3Au/5ZnO−ZrO$_2$, and 3Au/10ZnO−ZrO$_2$ catalysts at different ZnO amounts (3, 5, and 10 wt. %), thermally treated under air atmosphere at 200 °C; and (**E**) temporal stability for 24 h for 3Au/5ZnO−ZrO$_2$ at 10 °C using 40 mg of catalyst under dry conditions.

2.6.2. Effect of Using Hydrogen or Air in the CO Oxidation

The effect of the gas used in the thermal treatment of the catalysts with either air or hydrogen was tested for the 3Au/ZrO$_2$, 3Au/ZnO, and 3Au/5ZnO−ZrO$_2$ catalysts at 200 and 500 °C, respectively (see Figure 8A,B). In this sense, earlier reports have shown that samples synthesized by the method of deposition-precipitation with urea have resulted in Au^{3+} species that can be reduced in air or hydrogen toward Au^0 through different steps [33]. It is shown in Figure 8A,B that the activity displayed by the 3Au/5ZnO−ZrO$_2$ catalysts was higher than the activity displayed by those supported on single oxides when the samples were thermally treated in hydrogen and air at 200 °C, reaching 78% and 86% conversion at 0 °C, respectively. As for the 3Au/5ZnO−ZrO$_2$ catalysts, they were also treated in hydrogen and air at 500 °C (Figure 8A,B). In this case, the CO conversion decreased notably with regard to the same samples treated at 200 °C, reaching 19% and 42% conversion at 0 °C, respectively. In this way, the thermal treatment at 500 °C affects the properties of the 3Au/5ZnO−ZrO$_2$ catalyst, mainly modifying the gold particle size, morphology, and metal dispersion.

In Figure 8C, the effect of the gas hourly space velocity (GHSV) is shown for the most active 3Au/5ZnO−ZrO$_2$ catalyst using 20 and 40 mg of catalyst, representing a GHSV of 89,000 h^{-1} and 46,000 h^{-1}, respectively. The results revealed that at 0 °C, with a GHSV of 89,000 h^{-1}, the 3Au/5ZnO−ZrO$_2$ catalysts showed acceptable activity, reaching 26% CO conversion, while at 46,000 h^{-1}, an increase in the CO oxidation was observed, displaying 86% CO conversion from 0 °C; likewise, it was preserved up to 300 °C, indicating that the 3Au/5ZnO−ZrO$_2$ catalyst presented superior performance in the CO oxidation with a GHSV of 46,000 h^{-1}.

2.6.3. Impact of the ZnO-ZrO$_2$ Composition

A positive catalytic promotion when ZnO was added to ZrO$_2$ was observed (Figure 8D). The highest CO conversion was obtained by the 3Au/5ZnO−ZrO$_2$ catalyst, showing 86% CO conversion at −5 °C, while the 3Au/10ZnO−ZrO$_2$ and 3Au/3ZnO−ZrO$_2$ catalysts achieved CO conversions of 68% and 50% at 0 °C, respectively. The outcomes revealed that the addition of zinc (3, 5, and 10 wt. %) to ZrO$_2$ delayed the formation of the tetragonal structure, stabilizing the gold nanoparticle size at 200 °C, reaching CO conversion from 0 °C that was higher than the one displayed by the catalysts supported on single ZrO$_2$ and ZnO. Earlier works on mixed oxides have highlighted that the phase composition of oxides affects the size of the gold particles, stabilizing their growth and obtaining, as a consequence, better performance in the catalytic activity for oxidation reactions [34]. The ZrO$_2$−ZnO mixed oxide was proven to increase the activity of gold nanoparticles from 0°C. Previous studies have reported that ZnO concentrations from 5 to 40 wt. % on ZrO$_2$ have shown good catalytic activity results in oxidation reactions [35]. On the other hand, Figure 8E shows that the 3Au/5ZnO−ZrO$_2$ catalyst, under air atmosphere at 200 °C, underwent slight deactivation during the first 120 min at a reaction temperature of 10 °C and then remained stable, displaying high stability for at least 24 h. On the other hand, the catalytic activity of the 3Au/ZnO−ZrO$_2$ catalyst for the CO oxidation was compared with other catalysts reported in the literature (see Table 4). As can be observed in Table 4, the 3Au/ZnO−ZrO$_2$ catalysts showed similar Ea values to those displayed by the Au/ZnO and Au/ZrO$_2$ catalysts, which have been previously reported.

Table 4. Comparison of CO oxidation catalysts.

Catalyst	Ea (kJ)	T_{90} (°C)	Au loading (wt. %)	Catalyst Mass (g)	Ref
Au/ZnO	23	150	1.0	0.2	[6]
Au/ZrO$_2$	20.3	160	4.9	0.050	[36]
Au/ZnO	18.29	170	2.0	0.040	[37]
Au/ZrO$_2$	18	110	3.0	0.25	[38]
3Au/5ZnO−ZrO$_2$	21.7	5	3.0	0.040	This work

3. Materials and Methods

3.1. Synthesis of the Nanostructured ZrO_2 and $ZnO-ZrO_2$ Oxides

ZrO_2 and $ZnO-ZrO_2$ supports were prepared by the sol–gel method. The zirconia and zinc-zirconia oxides were prepared using the following procedure: the required amounts of $Zn(NO_3)_2$ aqueous solution and 18 mL of zirconium(IV) propoxide (Aldrich 70%) were simultaneously added to a previously prepared solution containing 18 mL of distilled water and 100 mL of 2-propanol (Baker 99%). Subsequently, the gelling solution was refluxed at 80°C under constant stirring. The amounts of $Zn(NO_3)_2$ per zirconium(IV) propoxide were calculated to provide 3, 5, and 10 wt. % loadings of ZnO in the final ZnO-ZrO$_2$ mixed oxide; the samples were labeled as $3ZnO-ZrO_2$, $5ZnO-ZrO_2$, and $10ZnO-ZrO_2$. Bare sol–gel ZrO_2 was synthesized in a very similar manner. The gel was obtained through controlled hydrolysis-condensation reactions of zirconium propoxide at 70 °C for 24 h at pH close to 3 with HNO_3 and 18 mL of deionized distilled H_2O. Afterwards, the materials were evaporated in a rotary evaporator at 80 °C and then dried in an oven for 16 h at 80 °C. Finally, they were treated in static air at 500 °C for 4 h with a rate of 3 °C/min. As for ZnO, it was prepared by the precipitation method using $Zn(NO_3)_2$ and NaOH as precursors. The aqueous solutions of 0.3 M zinc nitrate ($Zn(NO_3)_2.6H_2O$) and 0.5 M NaOH were prepared with deionized H_2O. NaOH was added to the zinc nitrate solution at constant stirring, with a white suspension being formed immediately, which was centrifuged and washed several times with distilled H_2O, and then with absolute alcohol. The obtained material was annealed at 500 °C in air atmosphere for 4 h to produce the ZnO sample.

3.2. Synthesis of Au Nanoparticles on the ZrO_2, ZnO, and $ZnO-ZrO_2$ Oxides

Au nanoparticles were synthesized by the method of deposition-precipitation with urea. To this end, $HAuCl_4$ and urea were dissolved in distilled H_2O. The Au loadings were close to 1, 2, and 3 wt. %, and the samples were labeled as Au/ZrO$_2$, Au/ZnO, and Au/ZnO−ZrO$_2$. For the synthesis of the Au materials, 250 mg of ZrO_2, ZnO, and $ZnO-ZrO_2$ (dried at 80 °C) were added to the $HAuCl_4$ and urea solution under constant stirring; subsequently, the suspension temperature was increased and then maintained at 80 °C under constant stirring for 16 h. After the procedure of deposition-precipitation with urea, all the materials were centrifuged and washed several times with H_2O at 50 °C, and dried under vacuum for 2.5 h at 80 °C.

3.3. Catalytic Evaluation

In a flow reactor, the CO catalytic oxidation reaction was carried out at atmospheric pressure, using 40 mg of sample that was first activated in situ with 40 mL min^{-1} of either air or hydrogen with a heating rate of 2 °C min^{-1}, between 200 and 500 °C in a tubular reactor (ID = 0.001 m; L = 0.035 cm) with a porous quartz frit disk placed in the middle of the tube to support the catalyst, using an RIG−150 micro reactor system by In-Situ Research Instruments. The feed gas mixture (1 vol. % of CO and 1 vol. % of O_2 balanced with N_2) was introduced with a total flow rate of 100 mL min^{-1} and a heating rate of 2 °C min^{-1}. The gases were analyzed with an online gas chromatograph (GC) (7820A, Agilent Technologies) equipped with an FID detector.

3.4. In Situ Characterization Techniques

DRIFTS results of in situ CO oxidation were collected on an FTIR spectrometer (Nicolet iS50R FTIR) equipped with a Harrick DRIFT cell in the 400–4000 cm^{-1} interval with 128 scans at a resolution of 4 cm^{-1} using ZnSe windows. In a typical experiment, the powder samples were pretreated in air (40 mL min^{-1}) at 200 °C for 2 h to remove the residuals. After cooling down to 20 °C, a background spectrum was collected at 4 cm^{-1} resolution for 128 scans in N$_2$ atmosphere. Then, the reactant gas (1 vol. % of CO and 1 vol. % of O$_2$ balanced with N$_2$) was continuously introduced into the in situ reaction chamber and monitored through mass spectrometry (Hidden analytical HPR-20 R&D bench-top gas analysis system).

3.5. Ex Situ Characterization Techniques

X-ray diffraction patterns of the samples packed in a glass holder were recorded at room temperature with Cu Kα radiation in a Bruker Advance D-8 diffractometer, with a theta–theta configuration and a graphite secondary-beam monochromator. The data were collected for scattering angles (2θ) ranging from 4 to 80° with a step size of 0.01° for 2 s per point.

Transmission electron microscopy (TEM) images were obtained with a JEOL 2200FS microscope with accelerating voltage of 200 kV, equipped with a Schottky-type field emission gun and an ultrahigh-resolution pole piece (Cs = 0.5 mm, point-to-point resolution, 0.190 nm). The materials were dispersed in isopropyl alcohol and deposited on a 200 mesh copper grid covered with a perforated carbon film. BET surface area was obtained by nitrogen physisorption in an ASAP-2000 analyzer (Micromeritics).

H$_2$-TPR profiles were performed on a Micromeritics AutoChem II 2920 automated catalyst characterization system under flow of a 10% H$_2$/Ar gas mixture (25 mL min^{-1}) with a heating rate of 10 °C min^{-1}, from room temperature to 600 °C.

XPS spectra were obtained with a Thermo VG Scientific Escalab 250 spectrometer equipped with a hemispherical electron analyzer and an Al Kα radiation source (1486.6 eV) powered at 20 kV and 30 mA, respectively. The binding energy was determined by using carbon C (1s) as reference line (284.6 eV). The spectrometer was operated at a pass energy of 23.5 eV, and the base pressure in the analysis chamber was maintained in the order of 3 $\times$ 10^{-8} mbar. Deconvolution peak fitting was done by using XPSPEAK 41 with Shirley background.

4. Conclusions

The addition of ZnO to a ZrO$_2$ support of gold catalysts showed an improvement in the physicochemical characteristics and, overall, in the catalytic performance of CO oxidation at low temperature (-5 °C). Outcomes revealed that the specific surface area and reduction temperature of gold increased with the ZnO content. ZnO as catalyst support is not interesting in terms of reducibility and dispersion of metallic gold; however, its interaction with ZrO$_2$ helped notably increase the gold dispersion. Au/ZnO$-$ZrO$_2$ tested at 46,000 h^{-1} in the oxidation of CO showed maximal conversion of 86% at -5 °C. On the other hand, the increase in the ZnO content on ZrO$_2$ in the catalyst support decreased the CO oxidation; in this sense, it was proven that the combined presence of ZnO and ZrO$_2$ in the gold catalyst support is necessary to achieve higher reaction rates. Therefore, the key factors for the best catalytic activity may be the Zn/Zr ratio and the state of gold species on the mixed oxide support. Likewise, other parameters such as the homogeneity of the final mixed oxide, Au particles size, and ZnO–ZrO$_2$ interaction play a role in the CO oxidation reaction, which was corroborated with the help of DRIFTS-GC/MS. It was found that gold adsorbs CO more strongly from low temperatures on ZrO$_2$ and ZnO$-$ZrO$_2$ than on ZnO, suggesting that the reactive surface exhibits more active gold sites under air treatment at 200 °C.

References

1. Okumura, M.; Fujitani, T.; Huang, J.; Ishida, T. A Career in Catalysis: Masatake Haruta. *ACS Catal.* **2015**, *5*, 4699–4707. [CrossRef]
2. Christmann, K.; Schwede, S.; Schubert, S.; Kudernatsch, W. Model Studies on CO Oxidation Catalyst Systems: Titania and Gold Nanoparticles. *ChemPhysChem* **2010**, *11*, 1344–1363. [CrossRef]
3. Haruta, M.; Tsubota, S.; Kobayashi, T.; Kageyama, H.; Genet, M.J.; Delmon, B. Low-Temperature Oxidation of CO over Gold Supported on TiO_2, α-Fe_2O_3, and Co_3O_4. *J. Catal.* **1993**, *144*, 175–192. [CrossRef]
4. Chen, S.; Abdel-Mageed, A.M.; Hauble, A.; Ishida, T.; Murayama, T.; Parlinska-Wojtan, M.; Jürgen, B.R. Performance of Au/ZnO catalysts in CO_2 reduction to methanol: Varying the Au loading/Au particle size. *Appl. Catal. A Gen.* **2021**, *624*, 118318. [CrossRef]
5. Ishida, T.; Kinoshita, N.; Okatsu, H.; Akita, T.; Takei, T.; Haruta, M. Influence of the Support and the Size of Gold Clusters on Catalytic Activity for Glucose Oxidation. *Angew. Chem. Int. Ed.* **2008**, *47*, 9265–9268. [CrossRef]
6. Carabineiro, S.A.C.; Machado, B.F.; Bacsa, R.R.; Serp, P.; Dražić, G.; Faria, J.L.; Figueiredo, J.L. Catalytic performance of Au/ZnO nanocatalysts for CO oxidation. *J. Catal.* **2010**, *273*, 191–198. [CrossRef]
7. Ueda, A.; Oshima, T.; Haruta, M. Reduction of nitrogen monoxide with propene in the presence of oxygen and moisture over gold supported on metal oxides. *Appl. Catal. B Environ.* **1997**, *12*, 81–93. [CrossRef]
8. Al-Sayari, S.; Carley, A.; Taylor, S.; Hutchings, G. Au/ZnO and Au/Fe_2O_3 catalysts for CO oxidation at ambient temperature: Comments on the effect of synthesis conditions on the preparation of high activity catalysts. *Top. Catal.* **2007**, *44*, 123–128. [CrossRef]
9. Kołodziejczak-Radzimska, A.; Jesionowski, T. Zinc Oxide-From Synthesis to Application: A Review. *Materials* **2014**, *9*, 2833–2881. [CrossRef]
10. Qian, K.; Huang, W.; Fang, J.; Lv, S.; He, B.; Jiang, Z.; Wei, S. Low-temperature CO oxidation over $Au/ZnO/SiO_2$ catalysts: Some mechanism insights. *J. Catal.* **2008**, *255*, 269–278. [CrossRef]
11. Boccuzzi, F.; Chiorino, A.; Tsubota, S.; Haruta, M. FTIR study of carbon monoxide oxidation and scrambling at room temperature over gold supported on ZnO and TiO_2. *J. Phys. Chem.* **1996**, *100*, 3625–3631. [CrossRef]
12. Wang, G.Y.; Zhang, W.X.; Lian, H.L.; Jiang, D.Z.; Wu, T.H. Effect of calcination temperatures and precipitant on the catalytic performance of Au/ZnO catalysts for CO oxidation at ambient temperature and in humid circumstances. *Appl. Catal. A Gen.* **2003**, *239*, 1–10. [CrossRef]
13. Hutchings, G.J.; Siddiqui, M.R.H.; Burrows, A.; Kiely, C.J.; Whyman, R.J. High-activity Au/CuO–ZnO catalysts for the oxidation of carbon monoxide at ambient temperature. *Chem. Soc. Faraday Trans.* **1997**, *93*, 187–188. [CrossRef]
14. Sagar, T.V.; Zavašnik, J.; Finšgar, M.; Novak-Tušar, N.; Pintar, A. Evaluation of Au/ZrO_2 Catalysts Prepared via Post synthesis Methods in CO_2 Hydrogenation to Methanol. *Catalysts* **2022**, *12*, 218. [CrossRef]
15. Derrouiche, S.; La Fontaine, C.; Thrimurtulu, G.; Casale, S.; Delannoy, L. Unusual behaviour of Au/ZnO catalysts in selective hydrogenation of butadiene due to the formation of a AuZn nanoalloy. *Catal. Sci. Technol.* **2016**, *6*, 6794–6805. [CrossRef]
16. Liu, R.; Qin, Z.; Ji, H.; Su, T. Synthesis of Dimethyl Ether from CO_2 and H_2 Using a Cu–Fe–Zr/HZSM-5 Catalyst System. *Ind. Eng. Chem. Res.* **2013**, *52*, 16648–16655. [CrossRef]
17. Zhang, X.; Shi, H.; Xu, B.Q. Catalysis by Gold: Isolated Surface Au^{3+} Ions are Active Sites for Selective Hydrogenation of 1,3-Butadiene over Au/ZrO_2 Catalysts. *Angew. Chem. Int. Ed.* **2005**, *44*, 7132. [CrossRef]
18. Huang, H.Y.; Chen, H.I.; Huang, Y.J. The Promotional Effects of ZrO_2 and Au on the CuZnO Catalyst Regarding the Durability and Activity of the Partial Oxidation of Methanol. *Catalysts* **2018**, *8*, 345. [CrossRef]
19. Wei, S.; Wang, W.W.; Fu, X.P.; Li, S.Q.; Jia, C.J. The effect of reactants adsorption and products desorption for Au/TiO_2 in catalyzing CO oxidation. *J. Catal.* **2019**, *376*, 134–145. [CrossRef]

20. Bailey, S.; Froment, G.F.; Snoeck, J.W.; Waugh, K.C. A DRIFTS study of the morphology and surface adsorbate composition of an operating methanol synthesis catalyst. *Catal. Lett.* **1995**, *30*, 99. [CrossRef]

21. Medina, J.C.; Figueroa, M.; Manrique, R.; Rodríguez Pereira, J.; Srinivasan, P.D.; Bravo-Suárez, J.J.; Baldovino Medrano, V.G.; Jiménez, R.; Karelovic, A. Catalytic consequences of Ga promotion on Cu for CO_2 hydrogenation to metanol. *Catal. Sci. Technol.* **2017**, *7*, 3375. [CrossRef]

22. Kunkes, E.L.; Studt, F.; Abild-Pedersen, F.; Schlögl, R.; Behrens, M. Hydrogenation of CO_2 to methanol and CO on $Cu/ZnO/Al_2O_3$: Is there a common intermediate or not? *J. Catal.* **2015**, *328*, 43. [CrossRef]

23. Saussey, J.; Lavalley, J.C. An in situ FT-IR study of adsorbed species on a $Cu-ZnAl_2O_4$ methanol catalyst under 1 MPa pressure and at 525 K: Effect of the $H_2/CO/CO_2$ feed stream composition. *J. Mol. Catal.* **1989**, *50*, 343. [CrossRef]

24. Edwards, J.F.; Schrader, G.L. In Situ FT-IR Spectroscopy of the Adsorption of CO on Methanol Catalysts. *Appl. Spectrosc.* **1981**, *35*, 559. [CrossRef]

25. Edwards, J.F.; Schrader, G.L. Infrared spectroscopy of copper/zinc oxide catalysts for the water-gas shift reaction and methanol synthesis. *J. Phys. Chem.* **1984**, *88*, 5620. [CrossRef]

26. Moulder, J.F.; Stickle, W.F.; Sobol, P.E.; Bomben, K.D. *Handbook of X-ray Photoelectron Spectroscopy*; Chastain, J., Ed.; Perkin-Elmer Corporation, Physical Electronics Division: Chanhassen, MN, USA, 1992; ISBN 0-9627026-2-5.

27. NIST. *X-ray Photoelectron Spectroscopy Database*; Version 4.1; National Institute of Standards and Technology: Gaithersburg, MD, USA, 2000; Version 4.1, Last Update to Data Content: 2012.

28. Li, X.; Han, C.; Lu, D.; Shao, C.; Li, X.; Liu, Y. Highly electron-depleted $ZnO/ZnFe_2O_4/Au$ hollow meshes as an advanced material for gas sensing application. *Sens. Actuators B* **2019**, *297*, 126769. [CrossRef]

29. Bai, S.; Chen, L.; Chen, S.; Luo, R.; Li, D.; Chen, A.; Liu, C.C. Reverse microemulsion in situ crystallizing growth of ZnO nanorods and application for NO_2 sensor. *Sens. Actuators B Chemical* **2014**, *190*, 760–767. [CrossRef]

30. Villa, A.; Dimitratos, N.; Chan-Thaw, C.E.; Hammond, C.; Veith, G.M.; Wang, D.; Manzoli, M.; Prati, L.; Hutchings, G.J. Characterisation of gold catalysts. *Chem. Soc. Rev.* **2016**, *45*, 4953–4994. [CrossRef]

31. Gan, J.; Lu, X.; Wu, J.; Xie, S.; Zhai, T.; Yu, M.; Zhang, Z.; Mao, Y.; Wang, S.C.I.; Shen, Y. Oxygen vacancies promoting photoelectrochemical performance of In_2O_3 nanocubes. *Sci. Rep.* **2013**, *3*, 1021. [CrossRef]

32. Menegazzo, F.; Signoretto, M.; Damiano, M.; Pinna, F.; Manzoli, M. Structure–activity relationships of Au/ZrO_2 catalysts for 5-hydroxymethylfurfural oxidative esterification: Effects of zirconia sulphation on gold dispersion, position and shape. *J. Catal.* **2015**, *326*, 1–8. [CrossRef]

33. Corro, G.; Cebada, S.; Pal, U.; Fierro, J.L.G. Au^0–Au^{3+} bifunctional site mediated enhanced catalytic activity of Au/ZnO composite in diesel particulate matter oxidation. *J. Catal.* **2017**, *347*, 148–156. [CrossRef]

34. Ilieva, L.; Dimitrov, D.; Kolentsova, E.; Venezia, A.M.; Karashanova, D.; Avdeev, G.; Petrova, P.; State, R.; Tabakova, T. Gold-Based Catalysts for Complete Formaldehyde Oxidation: Insights into the Role of Support Composition. *Catalysts* **2022**, *12*, 705. [CrossRef]

35. Kim, M.Y.; Kamata, T.; Masui, T.; Imanaka, N. Complete Toluene Oxidation on Pt/CeO_2-ZrO_2-ZnO Catalysts. *Catalysts* **2013**, *3*, 646–655. [CrossRef]

36. Güttel, R.; Paul, M.; Galeano, C.; Schüth, F. Au,@ZrO_2 yolk–shell catalysts for CO oxidation: Study of particle size effect by ex-post size control of Au cores. *J. Catal.* **2012**, *289*, 100–104. [CrossRef]

37. Liu, W.; Liu, H.; Liu, Y.; Dong, Z.; Luo, L. Surface Plane Effect of ZnO on the Catalytic Performance of Au/ZnO for the CO Oxidation Reaction. *J. Phys. Chem. C* **2022**, *126*, 14155–14162. [CrossRef]

38. Konova, P.; Naydenov, A.; Tabakova, T.; Mehandjiev, D. Deactivation of nanosize gold supported on zirconia in CO oxidation. *Catal. Commun.* **2004**, *5*, 537–542. [CrossRef]